



Physics-informed machine learning model for battery state of health prognostics using partial charging segments

Sara Kohtz, Yanwen Xu, Zhuoyuan Zheng*, Pingfeng Wang*

Dept. of Industrial and Enterprise Systems Engineering, University of Illinois at Urbana-Champaign, Urbana, IL 61801, USA



ARTICLE INFO

Communicated by John E. Mottershead

Keywords:

Lithium-ion battery
State of health
Multi-fidelity model
Physics-informed machine learning
State estimation

ABSTRACT

The accurate and efficient estimation of battery state-of-health (SoH) is an ever-significant issue for applications of lithium-ion batteries (LIBs). Physics-of-failure (PoF) and machine-learning (ML) approaches have shown success in the field of prognostics and health management. However, accurate prediction of these models depends on clear understandings of complicated underlying physics, or full access to massive historical usage data of the system, which are not always obtainable in the engineering applications. Studies on physics-informed ML frameworks have gained attention because they embed physics knowledge into ML algorithms; recently, this method has demonstrated the potential to enhance performance over traditional model-based techniques, particularly when handling highly non-linear complex systems, such as LIBs. In this study, an advanced physics-informed ML (PIML) framework is proposed for the LIB SoH estimation, which includes three steps. The physics-based finite element (FE) model is firstly used to calculate the influences of the dominating aging mode, i.e., the solid electrolyte interface (SEI) growth on anode particle surfaces, and on capacity loss of LIB under various operating conditions. Then, the FE results are fused with experimental data from NASA Ames Prognostics Center of Excellence to construct a multi-fidelity model. Lastly, the Gaussian Process Regression (GPR) model is trained to create the mapping between voltage curves and the corresponding SEI thickness. A case study with the partial charging voltage segment as input is introduced to validate the PIML framework. Overall, the framework demonstrates a favorable performance for SoH estimation, as well as providing a basis for future online estimation frameworks.

1. Introduction

The lithium-ion batteries (LIBs) are one of the most widespread energy storage systems in modern society. In recent years, they have been rapidly expanding due to the ever-growing demands in various fields, such as smart grid systems, portable electronics, internet of things (IoT) devices, and hybrid/full electric vehicles (EV) [1-4]. Compared to other battery chemistries, LIBs have high energy/power densities and good cycle life performances [4,5], but the practical utilizations of LIBs and large battery packs require accurate state estimations. This is because, on one hand, the usage of batteries is restricted to the safe operating area (SOA), which depends on voltage, current and temperature, so that these parameters need to be carefully monitored to eliminate safety concerns [6,7]. On the other hand, the battery performances are influenced by the operating conditions, as well as various aging phenomena [8,9]. The states of LIBs that need to be estimated include state-of-charge (SoC), state-of-health (SoH), state-of-energy (SoE), etc. [10-

* Corresponding authors.

E-mail addresses: zhuoyuan@illinois.edu (Z. Zheng), pingfeng@illinois.edu (P. Wang).

[13], among which, enhancing the accuracy of SoH estimation is the most essential and fundamental [14].

Currently, different model-based approaches have been proposed to predict the LIB states, which can be mainly classified into physics-of-failure (PoF) based and data-driven approaches [15]. PoF-based models are grounded on first principles of the LIB system, which describe the multi-physics fields of the battery system and their couples, as well as its failure mechanisms. Luis et al. [15] developed a two-step approach for SoH estimation of a LIB to offer parameter-based indicators that characterize the long term evolution of the lithium ion diffusion and charge transfer processes associated to aging, and validated the experimental and simulation results of lithium iron phosphate (LFP) half battery cells. Qi et al. [16] reported a physics-based single particle model to simulate the life cycling data of a LIB and used the model to investigate the underlying mechanisms of capacity fade. In our previous studies, we investigated the influences of various failure modes, e.g., lithiation-induced stress, fracture and delamination of host electrode materials and unstable growth of solid electrolyte interface (SEI), on the performances of the silicon-based anode system via finite element analysis (FEA) [17-19]. However, the PoF based approaches are usually constructed based upon partial differential equation sets with unclear internal parameters, and can be difficult to derive for complex systems, especially when the operating/environmental conditions are noisy and uncertain; besides, high computational costs also limit the online applications of these approaches.

Aside from PoF based approaches, data-driven machine learning (ML) techniques are also widely used for the internal parameter prediction, fault/failure diagnosis, and prognostics and health monitoring of LIBs [20-26]. Various ML algorithms have been adopted to extract typical features from sensor data (e.g., voltage, current and temperature) to build the connections between operational data and system health; specifically, techniques such as extended Kalman filter (EKF) [27-30], support vector machines (SVM) [31], and artificial neural network (ANN) [32,33] have shown promising results. In addition, Selina et al. [20] proposed a naive Bayes (NB) model for remaining useful life (RUL) prediction of batteries; they found that the RUL of LIBs can be predicted with the NB method under constant discharge environments, and its robustness and accuracy were comparatively high irrespective of the exact values of the operating conditions. Yanzhou et al. [34] introduced a deep learning-based method to predict impedance spectra at the fully charged and fully discharged states over battery life using a convolutional neural network (CNN), which only required input data collected under constant-current charging; their results showed that the impedance spectra could be accurately predicted, along with the relaxation times and the extracted ohmic resistance. Jianbo [35] developed an ensemble learning model to integrate multiscale logic regression (LR) and Gaussian process regression (GPR) to tackle the SOH estimation problem; this design scheme could capture the time-varying degradation behavior and reduce the effects of local regeneration phenomenon in LIBs. Compared to physics-based models, the ML techniques can effectively and efficiently track the battery degradation and estimate its RUL; the implementation of these techniques are less complex and easier to employ into a real application. Nevertheless, the accuracy of these techniques depends crucially on the amount of historic data available and on the complexity of the system itself; in practical applications, there is little chance to acquire full charging/discharging curves of the LIBs, meanwhile the usage history of the batteries is often unknown. These scenarios could lead to a lack of data for conventional ML models. In addition, the models are not designed to reveal the underlying physics, which makes more difficult to improve their performances [22].

To overcome the aforementioned challenges, the physics-informed ML (PIML) methods have recently become more prevalent in the field of health management. PIML is an emerging research field with the concept of embedding physics principles into ML models [36,37]. This method has been adopted in many scientific applications, including weather forecasting, biological systems, materials chemistry, and mechanical failure. The emergence of PIML in diverse fields is due to its combined respective strengths of PoF-based and data-driven models; mainly, it can link information from physics and scattered noisy data, handle small data regime, and provide theoretical insight while elucidating inner mechanisms [38-40]. For example, Hao et al. [41] blended a single particle model with thermal dynamics (SPMT) with a feedforward neural network (FNN) to perform physics-informed learning of a LIB's dynamic behavior, which could provide considerable predictive accuracy. Muratahan et al. [42] outlined several potential architectures for integrating physics-based and machine learning models that could forecast battery lifetime, and discussed the ease of implementation, advantages, limitations and viability of each architecture.

In this study, we propose a PIML based multi-fidelity model for battery state of health (SoH) prognostics, which only uses flexible partial charging segment (less than 300 s' data) under constant current (CC) charging as the input. A physics-based finite element (FE) model is firstly constructed to predict the capacity fading of a graphite-anode-based LIB under different C-rates and temperatures, where the capacity degradation is attributed to the growth of solid electrolyte interface (SEI) on the anode surface. The experimental results on LIB data from NASA Ames Prognostics Center of Excellence are then used to validate the FE model, meanwhile a multi-fidelity model based upon the co-kriging algorithm is developed to combine the experimental and simulation results and create the mapping between capacity loss and the thickness of SEI. Afterwards, the Gaussian Process Regression (GPR) models are employed using FE results as training data to estimate the remaining capacity of the LIB, where the partial charging voltage segment and the operating temperature are used as the input. The training, validation, and testing of the PIML model are conducted on the NASA LIB data, indicating that the algorithm can estimate the battery SoH with less than 2% error.

The remaining of the paper is organized as follows. Section 2 introduces the development and implementation of the PIML based multi-fidelity model to predict the SEI thickness and battery SoH. Section 3 presents and discusses the numerical results. Finally, section 4 concludes the paper by summarizing significant remarks.

2. Modeling approach

In this section, the framework of the PIML based multi-fidelity model for SoH estimation is firstly explained. The physics-based FE model is then detailed to calculate the capacity degradation of the LIB caused by the SEI growth on the anode particle surfaces. A co-kriging based multi-fidelity model is introduced to directly project the SEI thickness to the SoH of the battery. And a Gaussian Process

regression (GPR) model is established for the SEI thickness estimation given partial charging voltage segment.

2.1. PIML-based multi-fidelity framework

Fig. 1 illustrates the architecture of the PIML-based multi-fidelity framework for battery SoH estimation. The framework consists of three major parts: 1) the physics-based 1D FE model (circled in red), 2) the GPR model (circled in green), and 3) the multi-fidelity model (circled in purple). In the 1st step, the physics-based FE model is used to calculate the capacity loss of the LIB induced by the SEI growth on the surfaces of anode particles under constant current charging protocol, where the influences of ambient temperature and charging C-rate have been taken into consideration. Secondly, the voltages curves, SEI thickness change, and battery capacity degradation with respect to the increasing cycle number are predicted. Then, the GPR models are constructed using the FE simulation results as the training data, and the mapping from battery operating conditions (temperature and C-rate) and voltage curve to the SEI thickness is created.

Once the model structure is determined, a case study is employed to demonstrate the feasibility of the PIML model, where the partial charging voltage segment are imported in the learned GPR model as input to predict the corresponding SEI thickness as output. Eventually, the co-kriging-based multi-fidelity model are developed based on the experimental data from NASA Ames Prognostics Center of Excellence and the FE simulation results; and the predicted SEI thickness from previous step is imported to estimate the SoH of the LIB. Note that, different from a conventional data-driven ML model, which attempted to directly predict the battery SoH using the sensor data, the architecture of the proposed PIML framework is advanced and arranged depending on the physical information and knowledge, that is, the dominating factor to battery aging performance is the accumulation of SEI layer [43,44]. In other words, with the change of SEI thickness and battery degradation status, the transient dynamics of the battery during the charging and discharging processes also vary. Accordingly, one critical internal variable of the LIB system, i.e., the SEI layer thickness, is predicted as a mediate step to help adjust the prediction and improve the performances of model without increasing the computational burden. As a result, since the ML model is informed and restricted by the electrochemical physics, it is expected this method could tackle the highly non-linear problem and bring high accuracy, especially for quick SoH prognostics when the access to the testing data is limited. In the following sections, the development and implementation of these models are discussed.

2.2. Physics-based 1D FE model

Block 1 of **Fig. 1** shows the structure of the physics-based FE model, which is the first step in the proposed PIML methodology. In this study, the anode material of the LIB is assumed to be graphite particles. The aging phenomena in the LIB is primarily attributed to the growth of solid electrolyte interface (SEI) on the surfaces of anode particles in the charging-discharging cycles. In particular, due to the volumetric expansion of the graphite particles during lithiation process, the SEI layers that originally cover the anode may be cracked, resulting in the extra exposure of anode surfaces and additional formation of SEI [45]. The transportation flux of lithium-ion within the electrode material particle, J , is determined by the concentration gradient obeying Fick's law (1):

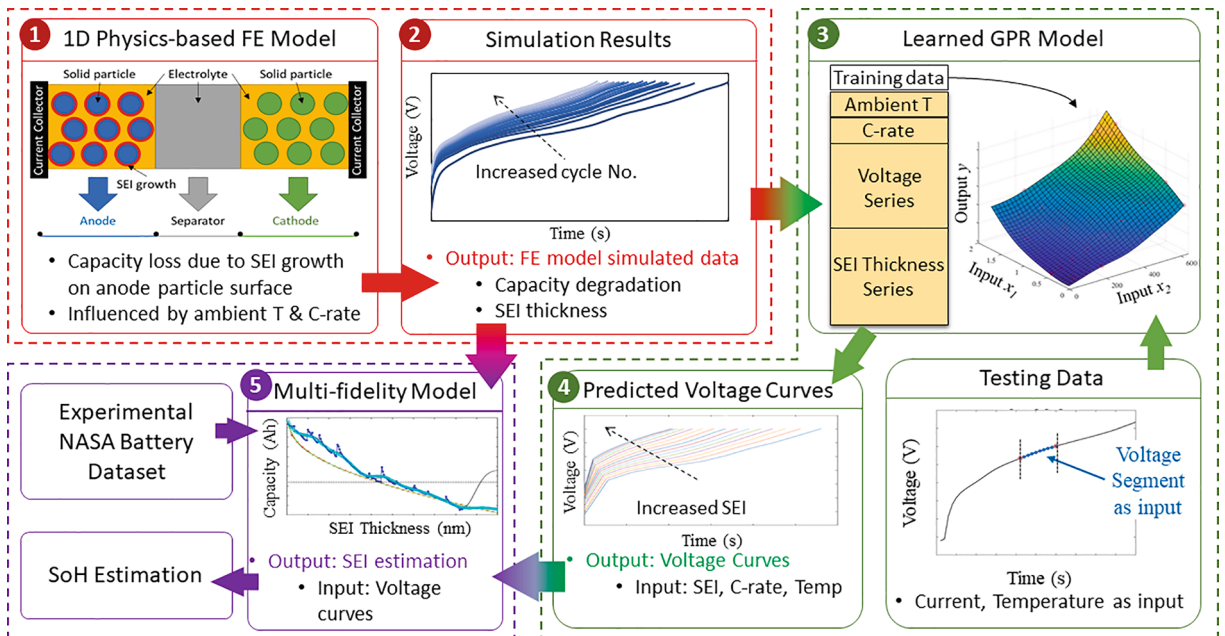


Fig. 1. Framework of the PIML-based multi-fidelity model for battery SoH estimation.

$$\mathbf{J} = -D\nabla c \quad (1)$$

where, c is the concentration of lithium, D is the diffusion coefficient, and ∇ is gradient operator. Further combining the transportation flux term (1) with the mass conservation equation, $\partial c/\partial t + \nabla \cdot \mathbf{J} = 0$, we have

$$\partial c/\partial t - D\nabla(\nabla c) = 0 \quad (2)$$

The boundary condition of Eq. (2) at the electrode–electrolyte surface is controlled by the electric current density I_n :

$$\mathbf{J} \cdot \mathbf{n} = I_n/F \quad (3)$$

where, \mathbf{n} is the normal vector of the electrode–electrolyte surface, and $F = 96485\text{C/mol}$ is the Faraday's constant. The electric current density I_n obeys the Butler–Volmer kinetics (4):

$$I = I_0[\exp(\alpha_a zF\eta/RT) - \exp(\alpha_c zF\eta/RT)] \quad (4)$$

where, I_0 is exchange current density, T is temperature, F is Faraday's constant, R is universal gas constant, α_c and α_a are the cathodic and anodic charge transfer coefficient, respectively, and η is the overpotential.

In addition, the current of the parasitic SEI forming reactions I_{SEI} is calculated via Eq. (5) [45]:

$$I_{\text{SEI}} = -(1 + HK_{\text{crl}}) \frac{J \cdot I}{\exp(\frac{\alpha_{\text{SEI}} F}{RT}) + \frac{Q_{\text{SEI}} f}{I}} \quad (5)$$

where, α , J , f and H are the fitting parameters related to the volumetric changes of the graphite particles; their values are functions of operating temperature, which are fitted with experimental results and cited from reference [45]. The accumulated capacity loss Q_{SEI} due to side reactions forming the SEI layer can then be defined as

$$\frac{dQ_{\text{SEI}}}{dt} = -I_{\text{SEI}} \quad (6)$$

And the SEI layer thickness s is proportional to Q_{SEI} according to

$$s = \frac{Q_{\text{SEI}} V}{(1 - \varepsilon_{\text{anode}}) A} \quad (7)$$

where, V is the coulombic volume of the SEI layer, i.e., the volume of formed SEI layer per passed charge of the reaction, $\varepsilon_{\text{anode}}$ is the solid phase volume fraction of the anode phase, and A is the surface area of the graphite particles. The other used electrochemical parameters are summarized in Table 1. Block 2 of Fig. 1 indicates the simulation results from the described physics model.

2.3. Gaussian process regression (GPR) model

The GPR surrogate model is developed to link the charging voltage curves with the SEI layer thickness based on a set of training sample points and then used to output the system performances, this is shown in blocks 3–4 of Fig. 1. Essentially, given the inputs of operating and charging C-rate, the voltage curves at unobserved points are the outputted. A general Kriging model can be expressed as

$$G_K(\mathbf{x}) = T(\mathbf{x}) + S(\mathbf{x}) \quad (8)$$

where $G_K(\mathbf{x})$ represents the prediction result of performance function at point \mathbf{x} using the Kriging model, trend function $T(\mathbf{x})$ is a polynomial term of \mathbf{x} that interpolates the input sample points, and $S(\mathbf{x})$ is a Gaussian stochastic process with zero mean and variance σ_2 . The polynomial term $f(\mathbf{x})$ is the product of two vectors, including the set of regression basis functions f and the regression coefficients β ,

$$T(\mathbf{x}) = f^T(\mathbf{x})\beta \quad (9)$$

The covariance function between arbitrary two input points \mathbf{x}_i and \mathbf{x}_j can be defined as

Table 1
Summary of the electrochemical parameters used in the FE model.

Parameters	Value
Lithium diffusion coefficient in graphite particle D_{Li}	$1.45 \times 10^{-13} \text{ m}^2/\text{s}$
Electrical conductivity σ	100 S/m
Radius of graphite particle r	2.5 μm
Solid phase volume fraction of the anode phase $\varepsilon_{\text{anode}}$	0.384
Exchange current density I_0	0.96 A/m ²
Graphite maximum capacity c^{max}	31507 mol/m ³
Coulombic volume of the SEI layer V	$1.04 \times 10^{-9} \text{ m}^3/\text{C}$
Graphite particles surface area A	78.5 μm^2

$$\text{Cov} [S(\mathbf{x}_i), S(\mathbf{x}_j)] = \sigma^2 \mathbf{R} (\mathbf{x}_i, \mathbf{x}_j) \quad (10)$$

where $\mathbf{R}(\mathbf{x}_i, \mathbf{x}_j)$ denotes the correlation function matrix and can be defined as

$$\mathbf{R}(\mathbf{x}_i, \mathbf{x}_j) = \text{Corr}(\mathbf{x}_i, \mathbf{x}_j) = \exp \left[- \sum_{p=1}^N a_p |x_i^p - x_j^p|^{b_p} \right] \quad (11)$$

where a_p and b_p are parameters of the Kriging model.

With n observations $O = [X, Y]$, where X is the input data set and Y is the input performance, the log-likelihood function of the Kriging model can be expressed as

$$\ln L = -\frac{1}{2} \left[n \ln(2\pi) + n \ln \sigma^2 + \ln |\mathbf{R}| + \frac{1}{2\sigma^2} (\mathbf{Y} - \mathbf{F}^T \boldsymbol{\beta})^T \mathbf{R}^{-1} (\mathbf{Y} - \mathbf{F}^T \boldsymbol{\beta}) \right] \quad (12)$$

where F is the regression basis function at X and $F_{ij} = f_j(x_i)$. Then $\boldsymbol{\beta}$ and σ_2 can be solved by maximizing the likelihood function respectively, as

$$\boldsymbol{\beta} = [\mathbf{F}^T \mathbf{R}^{-1} \mathbf{F}]^{-1} \mathbf{F}^T \mathbf{R}^{-1} \mathbf{Y} \quad (13)$$

$$\sigma^2 = \frac{(\mathbf{Y} - \mathbf{F}^T \boldsymbol{\beta})^T \mathbf{R}^{-1} (\mathbf{Y} - \mathbf{F}^T \boldsymbol{\beta})}{n} \quad (14)$$

where n is the number of samples.

With the Kriging model, the response for any given new point \mathbf{x}' can be estimated as

$$G_K(\mathbf{x}') = \mathbf{f}^T \boldsymbol{\beta} + \mathbf{r}^T \mathbf{R}^{-1} (\mathbf{Y} - \mathbf{F}^T \boldsymbol{\beta}) \quad (15)$$

where \mathbf{r} is the correlation vector between \mathbf{x}' and the sampled points X . The mean square error $e(\mathbf{x}')$ can be computed by

$$e(\mathbf{x}') = \sigma^2 \left[1 - \mathbf{r}^T \mathbf{R}^{-1} \mathbf{r} + \frac{(1 - \mathbf{r}^T \mathbf{R}^{-1} \mathbf{r})^2}{\mathbf{F}^T \mathbf{R}^{-1} \mathbf{F}} \right] \quad (16)$$

Thus, the prediction of the response value at the new sample point \mathbf{x}' using the Kriging model can be considered as a random variable that follows a normal distribution with mean $G_K(\mathbf{x}')$ and variance $e(\mathbf{x}')$.

2.4. Co-kriging based multi-fidelity model

The Co-kriging based multi-fidelity model, indicated in block 5 of Fig. 1, is used to bridge the gap between the SEI thickness variable and the battery SoH. For Li-Ion batteries, as the SEI thickness increases, the capacity decreases and this relationship is captured with the co-kriging formulation. Co-kriging is a multivariate extension of Kriging, fusing information from multiple fidelity levels of data together. Essentially, there are two models with different fidelity levels, and the low-fidelity model is embedded within the high-fidelity model, as shown in Equation (17). The high-fidelity estimate can be found as the sum of two Gaussian processes, including the low-fidelity Kriging model, $G_{low}(\mathbf{x})$, and the Kriging model of the discrepancy model the difference between high-fidelity and low-fidelity information, $G_{diff}(\mathbf{x})$. In this study, the NASA experimental data and FE simulation results are treated to be the high-fidelity and low-fidelity information, respectively. The subscripts “low” and “diff” denote “low-fidelity” and “discrepancy” models, respectively. In general, a two-level Co-Kriging model is

$$G_{CoK}(\mathbf{x}) = \rho G_{low}(\mathbf{x}) + G_{diff}(\mathbf{x}) \quad (17)$$

where ρ is a scaling factor. $G_{low}(\mathbf{x})$ and $G_{diff}(\mathbf{x})$ are constructed using the Kriging method described in the previous section. The Co-Kriging predictor is written as

$$G_{CoK}(\mathbf{x}) = \mathbf{f}^T \boldsymbol{\beta} + \mathbf{r}_{CoK}^T \mathbf{R}_{CoK}^{-1} (\mathbf{Y}_{CoK} - \mathbf{F}^T \boldsymbol{\beta}) \quad (18)$$

Denote the low-fidelity and high-fidelity outputs as

$$\mathbf{Y}_{CoK} = \begin{pmatrix} Y_{low} \\ Y_{high} \end{pmatrix} = \begin{pmatrix} y_{low}(x_{low}) \\ y_{high}(x_{high}) \end{pmatrix} \quad (19)$$

where x_{low} and x_{high} represent the low-fidelity and high-fidelity inputs, respectively. Then, the covariance vector (\mathbf{r}_{CoK}) and matrix (\mathbf{R}_{CoK}) are

$$\mathbf{r}_{CoK} = \begin{pmatrix} \rho \sigma_{low}^2 \mathbf{r}_{low}(x_{low}, x) \\ \rho^2 \sigma_{low}^2 \mathbf{r}_{low}(x_{high}, x) + \sigma_{diff}^2 \mathbf{r}_{diff}(x_{high}, x) \end{pmatrix} \quad (20)$$

$$R_{CoK} = \begin{pmatrix} \sigma_{low}^2 \mathbf{R}_{low}(x_{low}, x_{low}) & \rho \sigma_{low}^2 \mathbf{R}_{low}(x_{low}, x_{high}) \\ \rho \sigma_{low}^2 \mathbf{R}_{low}(x_{high}, x_{low}) & \rho^2 \sigma_{low}^2 \mathbf{R}_{low}(x_{high}, x_{high}) + \sigma_{diff}^2 \mathbf{R}_{diff}(x_{high}, x_{high}) \end{pmatrix} \quad (21)$$

The regression coefficient β is the sum of the low-fidelity and difference models, and the regression basis functions are

$$\beta = \beta_{low} + \beta_{diff} \quad (22)$$

$$F = \begin{pmatrix} F_{low} \\ F_{diff} \end{pmatrix} = \begin{pmatrix} f_{low}(x_{low}) \\ f_{diff}(x_{diff}) \end{pmatrix} \quad (23)$$

Similar to the Kriging model, the variance of the low-fidelity and discrepancy models are

$$\sigma_{low}^2 = \frac{(Y_{low} - F_{low}^T \beta_{low})^T \mathbf{R}_{low}^{-1}(x_{low}, x_{low})(Y_{low} - F_{low}^T \beta_{low})}{n_{low}} \quad (24)$$

$$\sigma_{diff}^2 = \frac{(Y_{diff} - F_{diff}^T \beta_{diff})^T \mathbf{R}_{diff}^{-1}(x_{high}, x_{high})(Y_{diff} - F_{diff}^T \beta_{diff})}{n_{high}} \quad (25)$$

where $Y_{diff} = Y_{high} - \rho Y_{low}$.

The Co-Kriging mean square error estimate is defined as

$$e(\mathbf{x}') = \rho \sigma_{low}^2 + \sigma_{diff}^2 + \frac{(1 - F^T \mathbf{R}_{CoK}^{-1} \mathbf{r})^2}{F^T \mathbf{R}_{CoK}^{-1} F} - \mathbf{r}_{CoK}^T \mathbf{R}_{CoK}^{-1} \mathbf{r}_{CoK} \quad (26)$$

2.5. Implementation for SEI estimation

The SEI thickness is a direct indicator of the capacity in LIBs. As the battery ages, the SEI thickness increases, and the capacity decreases. Additionally, full charging voltage cycles can show this growth in SEI thickness over multiple curves. In general, an aged

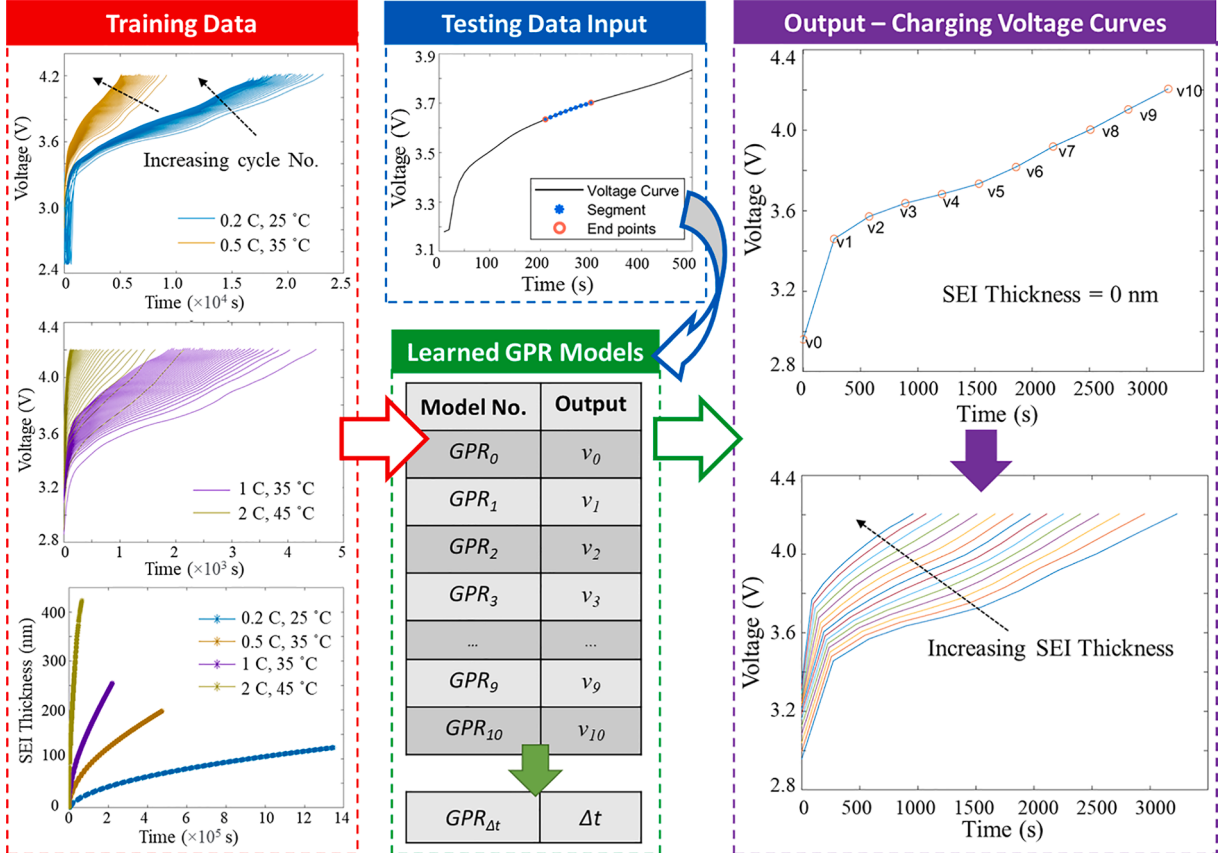


Fig. 2. Framework of GPR models for SEI estimation.

battery will complete a full charging cycle at a much faster rate than a newer battery, which would signify a high SEI thickness and a low capacity. Furthermore, a voltage curve with a specific shape and time can be generalized to specific SEI thickness levels. From the FE simulation results, the range of values for SEI thickness is from 0 to 425; in addition, the remaining capacity of the LIB is less than 50% when the SEI thickness is at 425 nm. Consequently, we define SEI levels from 0 to 425 nm with a step size of 1 nm, in order to estimate the charging behaviors of the LIB with various initial degradation conditions. Fig. 2 shows training data cycles; as the battery degrades, the SEI thickness increases, and the time to full charge decreases. Overall, different SEI thickness levels cause various voltage curves, and this connection is captured with the provided framework.

The model implementation for SEI estimation is summarized in Fig. 2. The training data generated from the previous section contains 15 scenarios that are defined as the charging and discharging curves under constant current protocol at given C-rates and ambient temperatures. In total, the training data consists of 3 different ambient temperatures (25°C , 35°C , 45°C) and 5 different discharge C-rates (0.2 C – 2.43 Amps, 0.33 C – 4.01 Amps, 0.5 C – 6.08 Amps, 1 C – 12.16 Amps, 2 C – 24.31 Amps) for a total of 15 different SEI escalation curves; 4 of which are shown as an example in the insets of Fig. 2. The main idea of this methodology is to capture the increased “steepness” of the voltage charging curve as an indicator to the battery’s SEI level. Hence, during testing, a full voltage curve is generated for each defined SEI level, then a similarity analysis would identify the voltage curve that best resembles the SEI level. This will enable the model to predict the SEI thickness of a singular voltage charging segment with no previous data on the battery’s history.

The procedure for training this part of the model starts by determining Gaussian process regression models (GPR) for a series of voltage points within a charging curve; i.e., obtaining $(v_0, v_1 \dots v_{10})$. Each GPR predicts one v ; as well as one extra GPR predicting Δt within the voltage curve. The objective is to generate a full voltage charging curve for each SEI level given parameters (current and temperature) from the testing segment. Subsequently, the voltage curve that is most similar to the testing segment indicates the SEI level of that particular segment. Due to the different time lengths of each cycle, both in the testing and training datasets, the estimation of Δt is a crucial step. In essence, within the training dataset, each full charging curve is normalized to be on the same time frame. The GPRs take as inputs the current, temperature and SEI thickness, then outputs its respective voltage point. Afterwards, the voltage points serve as inputs into the GPR that predicts Δt . The combination of voltage points and the predicted total time generated by each GPR allows for the creation of an entire voltage charging curve. The generated voltage curves for a given set of the SEI levels is shown at the end of Fig. 2.

Fig. 3 shows the process for estimating the SEI thickness given a singular partial charging segment. From this segment, the independent parameters of current and temperature are inputted into each GPR; as well as a distinct SEI level ($SEI_1, SEI_2 \dots SEI_{425}$). Since there are 425 “levels” of SEI thickness, there are 425 generated voltage charging curves (a subset of these curves is shown in Fig. 3); the total time for each charging curve is also predicted by $GPR_{\Delta t}$. The testing segment provides the values for the voltage window, as well as the total time within that particular segment. For example, in Fig. 3, the endpoints of the voltage testing segment are observed as 3.62 V and 3.73 V. After the formation of the voltage curves for each SEI level, the total time between 3.62 V and 3.73 V can be interpolated for each of these generated curves. Essentially, the voltage curve with the most similar interpolated total time to the test segment corresponds to the SEI level (this is shown as the “x” in the graph at the end of Fig. 3). Due to the possibility of multiple similar total times, a weighted sum of SEI estimations is taken as the final prediction; it is defined by the following equation:

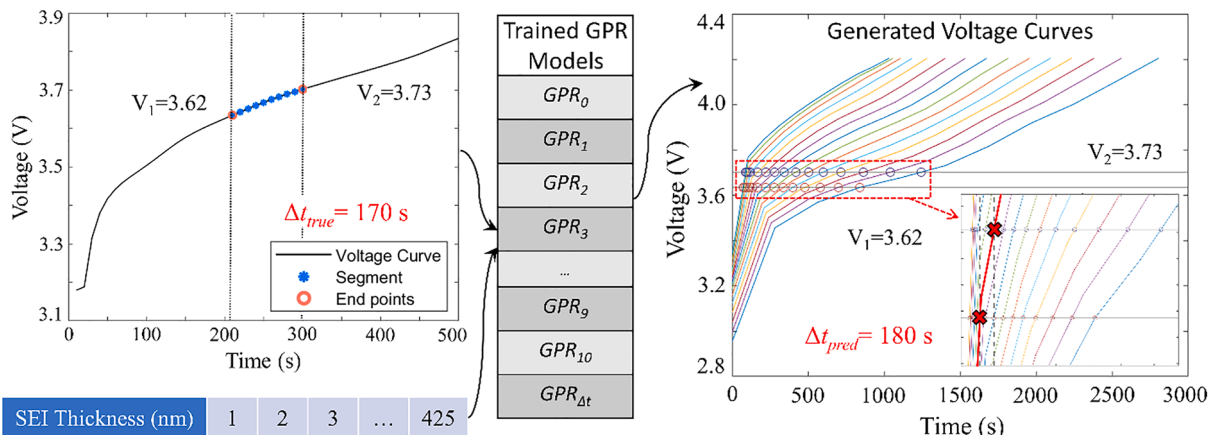


Fig. 3. Implementation of SEI estimation using partial charging segment.

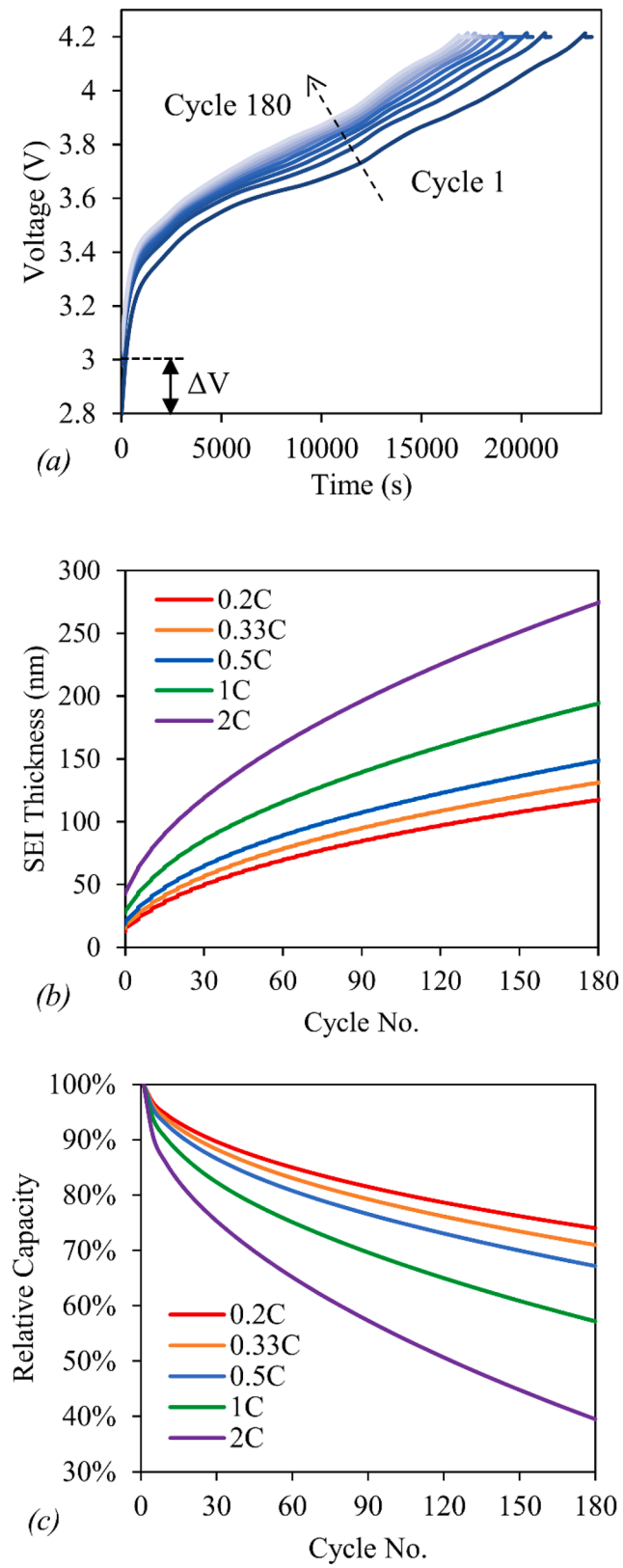


Fig. 4. (a) Simulated charging voltage curves of the LIB from cycle 1 to cycle 180 under 0.2 C-rate and 25C condition. Simulated (b) SEI thickness and (c) relative capacity as a function of cycle No. at 25C.

$$\begin{aligned}
 SEI &= \frac{1}{W} \sum_{i=1}^5 w_i * SEI_i^{est} \\
 W &= \sum_{i=1}^5 w_i \\
 w_i &= \frac{1}{(T_i - T^a)^2}
 \end{aligned} \tag{29}$$

where T_i is the estimated total time of the segment, and T^a is the actual total time for the segment.

For model validation, a testing dataset is generated with the charging C-rate of 1.5C (18.24 Amps) and ambient temperature of 30 °C. These conditions fall within the range of the training dataset, but the training data does not take on these exact values for current and temperature. The voltage segments are taken from the testing charging curves at different points within the cycle. The segments are monotonically increasing subdivisions of a charging curve, each of which are around the same amount of time, between 150 and 400 s. Since not all cycles are of the same length, some of the segments have slightly different total times due to the adjustments made for each cycle. Overall, the objective of the combined GPRs is to generate voltage curves for each predefined SEI level; and then utilize the total time as a similarity criterion matching to the testing partial charging segment.

3. Results & discussion

In this section, the numerical results are presented. The FE simulation and co-kriging multi-fidelity results are firstly discussed. Successively, a case study with given partial charging segment under constant current charging is introduced to validate the PIML-based Multi-fidelity Model.

3.1. The FE simulation results

Fig. 4 presents one selected scenario of the FE simulation results as an example, with the ambient temperature of 25C. **Fig. 4a** shows the simulated charging voltage curves from cycle 1 to cycle 180 under 0.2C-rate. The LIB is charged from 2.8 V to 4.2 V under constant current protocol; with the increase of cycle number, the total charging time gradually decreases from 23509 s to 17262 s, suggesting the reduction of battery capacity. Besides, because of the SEI formation, the internal resistance of the battery is largely increased, leading to a great potential drop $\Delta V \approx 0.2$ V in the beginning of the charging process. Furthermore, as shown in **Fig. 4b-c**, the SEI thickness and relative capacity of the LIB with different C-rates are predicted. It can be observed that, the thickness of SEI layer increases as a function of cycle No.; for instance, at 0.2 C-rate, the SEI thickness is extended to around 118 nm; as a result, the remaining relative capacity of the battery is only 74.1%. When the battery is charged at higher C-rates or elevated temperatures, the SEI growth is significantly exaggerated due to the increase of parasitic reaction current I_{SEI} according to Eq. (5).

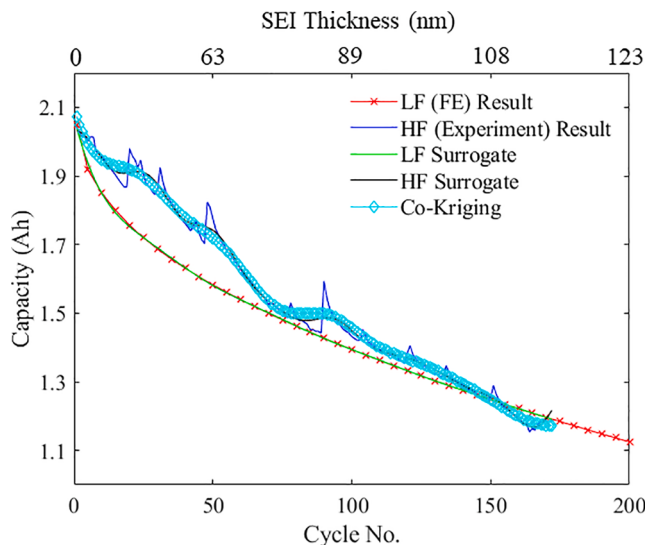


Fig. 5. Comparison of the LIB capacity as a function of cycle No. and SEI thickness among low-fidelity (LF) FE results, high-fidelity (HF) experimental data, LF surrogate model prediction, HF surrogate model prediction and Co-kriging model prediction.

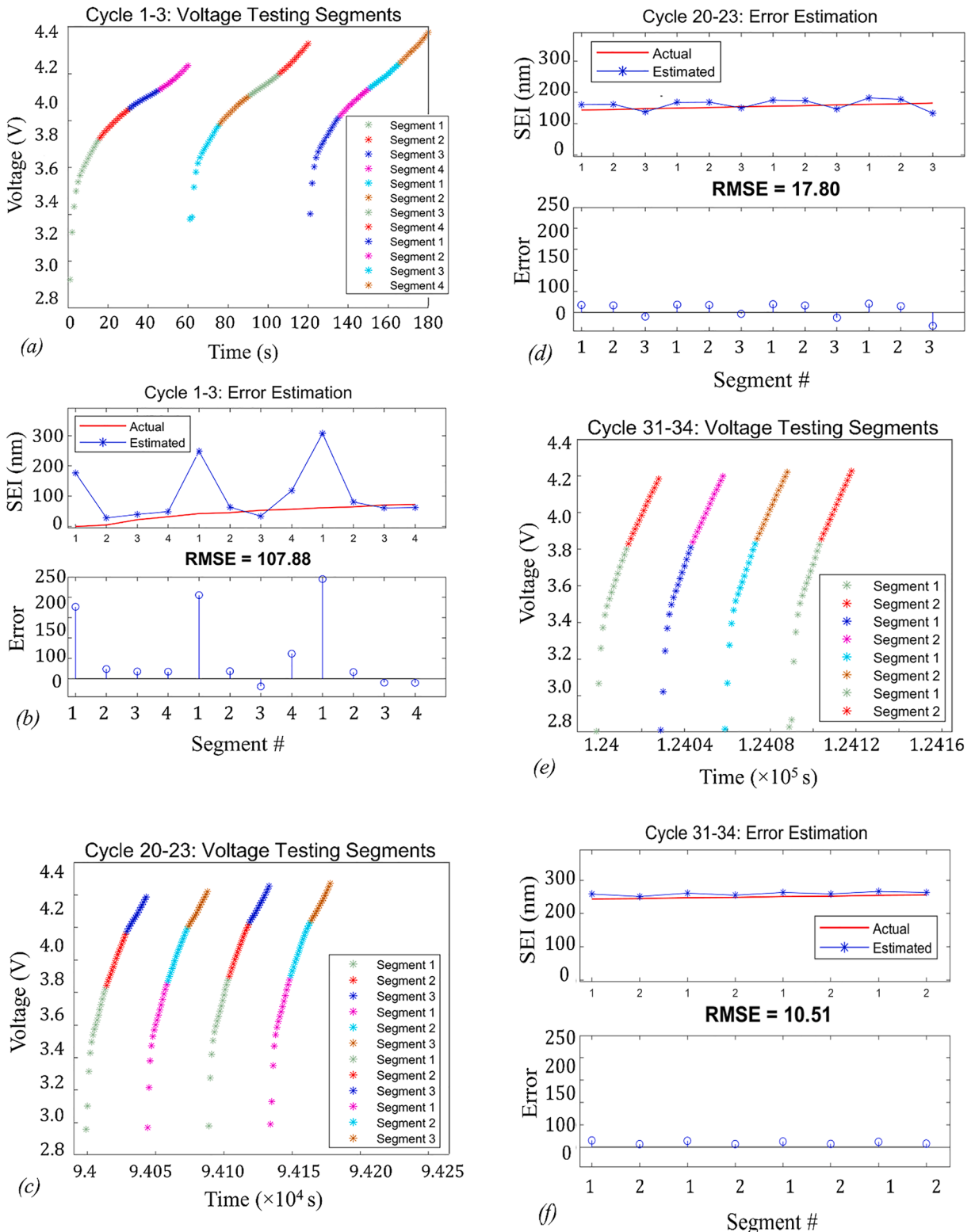


Fig. 6. Individual voltage testing segments and SEI estimations for (a-b) Cycles 1-3, (c-d) Cycles 20-23, and (e-f) Cycles 31-34.

3.2. Co-kriging multi-fidelity model

Co-kriging multi-fidelity model is adopted to provide accurate predictions of the LIB capacity with respect to the SEI thickness. Fig. 5 illustrates the comparison of the LIB capacity as a function of cycle No., as well as the SEI thickness, among low-fidelity (LF) FE simulation, high-fidelity (HF) experiment, LF surrogate model, HF surrogate model and Co-kriging model prediction. As can be seen, the physics-based FE model will slightly overestimate the capacity degradation of the battery, especially at lower cycle numbers. On the contrary, the co-kriging surrogate model could combine the experiments with FE results and calculate the error terms, therefore, shows the smallest error of 1.5%. In the following, the co-kriging model results will be utilized as the lookup table to estimate the SoH of the battery.

3.3. Validation and testing of the PIML-based multi-fidelity model

The estimation results of SEI thickness and prediction error using the PIML model with the selected cycles are presented in Fig. 6. Fig. 7 shows the summary of the SEI thickness estimation and error from all the tested partial charging segments. Since the estimations are based solely on partial charging segments, the x-axis is defined as the segment number. There is a total of 96 charging segments that are individually tested. The overall root mean squared error (RMSE) is 15.73. The model performs well at later cycles within the battery's health, but in the very early cycles, the error is quite high. This is because the initial segments define a lesser portion of the entire voltage curve (see cycle 1–3 in Fig. 6 a-b). These testing segments represent only a slight increase in voltage, and this smaller change in voltage has a higher likelihood of fitting to multiple different generated voltage curves. This suggests that for newer batteries, a longer testing segment would be needed for accurate SEI thickness estimation. As the battery ages and the cycles increase,

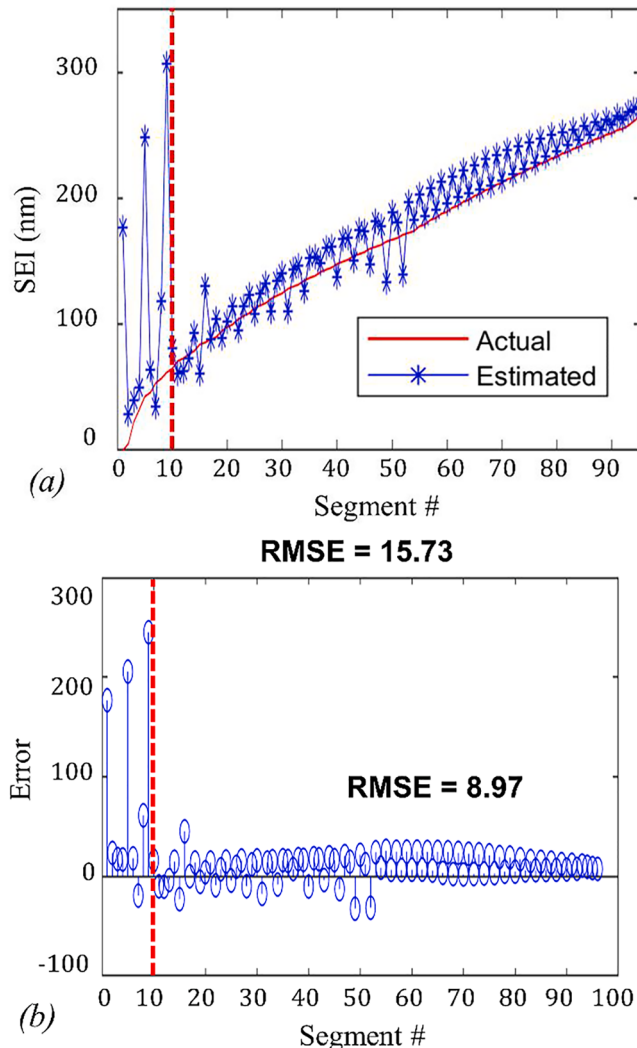


Fig. 7. Estimation of (a) SEI thickness and (b) prediction error for all the tested voltage segments.

more of the voltage charging curve is included within the segment, therefore the estimations are better. However, during practical applications, a battery that requires SoH prognostics is very likely to have experienced extensive utilizations. Consequently, the error in the early cycles can be ignored, which could reduce the RMSE is down to 8.97. Ultimately, the method provides satisfactory estimations of the SEI thickness level with just a partial charging segment.

In recent literature, there have been very few studies that utilize a partial voltage charging segment for estimation of SoH, and most of these scarce studies employ purely data-driven techniques. In addition, the segments taken as input to those models need to be quite large to obtain accurate results. For instance, Tian et al 2021 [46] utilizes a deep neural network to predict SoH given battery charging curve, however the segment requires over 10 min of data; while the method proposed in this paper takes inputs of segments between 150 and 400 s. For degraded Li-ion batteries, 10 min may be the time an entire charging cycle, so the reduction to 400 s is a significant improvement from practical standpoint. Other studies, such as Hosen et al 2021 [47] generate an entire (semi)-continuous voltage curve, which can be very error prone. In this paper, a nested GPR is utilized to predict discrete points within the voltage curve, and this much less prone to error; this is shown in Fig. 8, which compares GPR predicting continuous voltage curves as opposed to discrete points. Further justification for this rationale is provided in the discussion section.

As mentioned previously, there have been numerous studies regarding online estimation of SoH. The more successful ones utilize filtering frameworks, such as in [29,30]. The proposed methodology in this paper is unique in the sense that it can be incorporated into an online filtering framework. Filtering methodologies are a useful approach for online estimation, particularly for predicting SOH of Li-ion batteries. However, computational efficiency is very important for these methods, as most of these frameworks estimate the parameters and states concurrently, which means multiple variables are being updated given new observations. Therefore, careful consideration needs to be taken to ensure the online estimation framework is efficient enough to train the model and predict states. In this paper, the model is essentially static, meaning that all the training is completed offline. This provides an advantage since it does not have a strict requirement of computational efficiency. Still, some online updates (given observations) may be a promising future direction.

3.4. Discussion

The rationale behind the developed methodology stems from the objective of estimating the SEI thickness given a partial charging segment. Therefore, the novelty in the proposed framework lies in the physics-informed architecture. The advantages of this PIML is shown in two parts; the first has to do with training data, the second has to do with the framework of the nested GPR model, which is described in detail in Section 2. First, the FE model is developed to generate data and guide the GPR model, then it is utilized to extrapolate information from a very small amount of data (a partial charging segment). In recent literature, most SoH estimation methodologies assume some previous knowledge of the system to influence the algorithm's estimation, or at least have more informative inputs of data. Moreover, "clean" data is often an overlooked requirement for training machine learning models (clean referring to data with little to no noise); the FE model generates an abundance of "clean" data for training the nested GPR model. In addition, most of the online SoH estimation are in a recurrent framework, meaning the previous estimation output is utilized as an input for the next estimation. The proposed method utilizes the training data to generalize the observed parameters (voltage) with a given SoH level, therefore no previous knowledge is needed for accurate estimation. The ability to precisely estimate SoH given a voltage segment is particularly useful for health prognosis of repurposed battery pack cells. Since these cells have variable SoH levels, and the history of each cell is completely unknown, it would otherwise require the traditional coulomb counting process to determine the SoH level, which would take hours as opposed to minutes with the PIML algorithm.

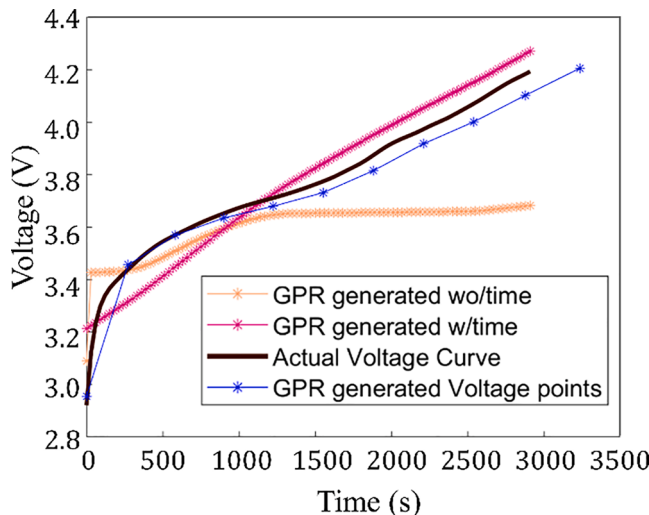


Fig. 8. Sample of GPR models for generated voltage curves. The actual voltage curve is taken as the first cycle in the testing dataset.

In addition, the architecture of the PIML model also shows the novelty of this study. Conventionally, a GPR model would be applied to estimate the SEI directly, with inputs defined as voltage, current, and temperature. While this would work with access to the battery's history, i.e., previous health estimations used as inputs, this simple structure does not work when estimating the SEI given an independent voltage segment. Therefore, a novel architecture is required for SEI estimation with no access to the battery's history, hence the concept of generating voltage curves is investigated. Fig. 8 compares the voltage prediction results via different structures, where the blue curve is the interpolated curve from the voltage points $(v_0, v_1 \dots, v_{10})$, and the dark brown curve is the target voltage curve. The other curves in Fig. 8 demonstrate the necessity of using multiple GPRs to generate voltage points, as opposed to a single GPR producing an entire voltage curve. The utilization of a singular GPR for voltage curve generation would simplify the model, however, it does not fit well to the target voltage curve. This is because a singular GPR can suffer from overfitting (as shown from the orange line) with the inputs as temperature, current and SEI level. The predicted voltage curve is improved when the time is given as an additional input, (as shown from the pink line), but this still does not fit well enough to capture the slight changes in voltage curve steepness due to increasing SEI levels. Moreover, regarding the problem statement, the testing segment's time points within the charging curve is unknown. This poses a substantial challenge, since, given a random partial charging segment, the endpoints could lie anywhere within the voltage curve. Therefore, the time-point within the voltage curve cannot be an input into the model. However, shown in Fig. 8, the pink line represents a GPR generated voltage curve with time as an input, and the orange line shows the GPR generated voltage curve without time. Noticeably, a singular GPR requires the input of time within a charging curve to be remotely close to the true voltage curve, which is not given in this application.

Ultimately, the method involving generating voltage points $(v_0, v_1 \dots, v_{10})$ and predicting the time between these points provides a close representation of the true voltage curve while satisfying the requirement of omitting time as an input. This enables the structure to predict an SEI thickness level based on the similarity between the voltage curves and the testing segment. Since voltage curves are being generated for each level of SEI, another aspect to consider is determining the most "similar" generated voltage curve with respect to the voltage segment, as this would identify the corresponding SEI level. This study also provides a novel method for identifying the corresponding SEI level. Typically, the use of a sliding window to obtain the distance between voltage segment and generated voltage curve would be the criterion, but by Fig. 8, the generated curves are not precise enough to capture the slight change in the voltage curve steepness. Thus, the similarity is defined between the total time of the testing segment and the interpolated total time of the testing segment's end points, as shown in Fig. 3. This similarity implementation is only possible when $GPR_{\Delta t}$ is trained and utilized, thus, this novel structure requires the utilization of multiple GPRs for generation of voltage curves and SEI prediction.

Further improvement may include determining where in charging curve a particular testing voltage segment lies. Since it is unknown where exactly in the voltage curve the segment is being sampled from, determining this information may further improve the estimation. From Fig. 3, the generated voltage curves for each SEI thickness level are much closer in distance at the beginning of a voltage curve, i.e., from (v_0, v_1) . Due to this closeness of voltage curves, it makes the methodology more prone to error. This is evident in the error plots in Fig. 6, where the high error comes from "Segment 1" of the charging cycle. One possible solution is to add another voltage point (another GPR) for the curve generation, i.e. $(v_0, v_{0.5}, v_1)$. This would enable generation of a more precise voltage curve. From any given voltage charging curve, at the start of the cycle, there is a steep increase, but the steepness can be better captured if more values between (v_0, v_1) are determined.

4. Conclusions

In summary, a novel framework of physics-informed machine learning with multi-fidelity model was proposed and demonstrated. The method was tested on the application of SoH estimation of LIBs and displayed accurate results. Additionally, while only a singular partial charging segment is required for SoH estimation, this method performed well with only a small amount of measurement data available. Since the multi-fidelity models and GPRs were trained and created offline, they could be implemented online for SoH estimation. This framework is beneficial for estimation of SoH for batteries with unknown history; specifically, cells that have been extracted from an electric vehicle battery-pack for potentially repurposing. Traditionally, extracting the SoH of LIBs would require a full discharge while being monitored with lab equipment (i.e., the coulomb counting method), which could take hours for a single battery cell. The PIML framework allows for SoH estimation in minutes. Overall, the physics-informed machine learning methodology provides an accurate and fast estimation for SoH than would otherwise be required given an unknown battery cell.

The remaining challenge with this framework is the storage of models and data to allow for online predictions of SoH. While the testing estimation is computationally efficient, the generated voltage curves still need to be stored. Future work includes developing a database to hold models and generated voltage curves of respective SEI/SoH levels. This process can be sped up if the testing segment parameters (i.e., current and temperature) remains consistent; however, for online SoH estimation of batteries in usage, this may not be possible, and it would be necessary to develop a more efficient version of this framework. For example, a future method may include determining a range of SEI values when first observing the testing segment, i.e., between 1 and 212 nm or 212–425 nm, then generate voltage curves for 212 values of SEI instead of 425; this would reduce the computational time. Other methodologies can be implemented to further reduce computational time and database byte storage. Conclusively, the PIML with multi-fidelity model is a novel framework that provides accurate predictions of SoH for LIBs; in addition, it provides a foundation for future methods of efficient online SoH estimations.

Declaration of Competing Interest

The authors declare that they have no known competing financial interests or personal relationships that could have appeared to

influence the work reported in this paper.

Acknowledgements

This work was partially supported by Office of Naval Research (ONR) through the Navy and Marine Corps Department of Defense University Research-to-Adoption (DURA) Initiative (N00014-18-S-F004), and the Engineering Research Center for Power Optimization of Electro-Thermal Systems (POETS) with cooperative agreement EEC-1449548.

References

- [1] N. Nitta, F.X. Wu, J.T. Lee, G. Yushin, Li-ion battery materials: present and future, *Mater. Today* 18 (2015) 252–264.
- [2] A. Raj, D. Steingart, Power sources for the internet of things, *J. Electrochim. Soc.* 165 (2018) B3130.
- [3] A. Mohd, E. Ortjohann, A. Schmelter, N. Hamsic, D. Morton, Challenges in integrating distributed energy storage systems into future smart grid. 2008 IEEE international symposium on industrial electronics, IEEE, 2008.
- [4] J.M. Tarascon, M. Armand, Issues and challenges facing rechargeable lithium batteries, *Nature* 414 (2001) 359–367.
- [5] M.T. McDowell, S.W. Lee, W.D. Nix, Y. Cui, 25th anniversary article: understanding the lithiation of silicon and other alloying anodes for lithium-ion batteries, *Adv. Mater.* 25 (2013) 4966–4984.
- [6] L. Lu, X. Han, J. Li, J. Hua, M. Ouyang, A review on the key issues for lithium-ion battery management in electric vehicles, *J. Power Sources* 226 (2013) 272–288.
- [7] K. Javed, R. Gouriveau, N. Zerhouni, State of the art and taxonomy of prognostics approaches, trends of prognostics applications and open issues towards maturity at different technology readiness levels, *Mech. Syst. Sig. Process.* 94 (2017) 214–236.
- [8] C. Hendricks, N. Williard, S. Mathew, M. Pecht, A failure modes, mechanisms, and effects analysis (FMMEA) of lithium-ion batteries, *J. Power Sources* 297 (2015) 113–120.
- [9] D.E. Acuña, M.E. Orchard, Particle-filtering-based failure prognosis via sigma-points: Application to lithium-ion battery state-of-charge monitoring, *Mech. Syst. Sig. Process.* 85 (2017) 827–848.
- [10] Q. Yu, R. Xiong, C. Lin, W. Shen, J. Deng, Lithium-ion battery parameters and state-of-charge joint estimation based on H-infinity and unscented Kalman filters, *IEEE Trans. Veh. Technol.* 66 (2017) 8693–8701.
- [11] X. Hu, J. Jiang, D. Cao, B. Egardt, Battery health prognosis for electric vehicles using sample entropy and sparse Bayesian predictive modeling, *IEEE Trans. Ind. Electron.* 63 (2015) 2645–2656.
- [12] X. Hu, S.E. Li, Y. Yang, Advanced machine learning approach for lithium-ion battery state estimation in electric vehicles, *IEEE Trans. Transp. Electrif.* 2 (2015) 140–149.
- [13] H. He, Y. Zhang, R. Xiong, C. Wang, A novel Gaussian model based battery state estimation approach: State-of-Energy, *Appl. Energy* 151 (2015) 41–48.
- [14] A. Smiley, G.L. Plett, An adaptive physics-based reduced-order model of an aged lithium-ion cell, selected using an interacting multiple-model Kalman filter, *J. Storage Mater.* 19 (2018) 120–134.
- [15] L.D. Couto, J. Schorsch, N. Job, A. Léonard, M. Kinnaert, State of health estimation for lithium ion batteries based on an equivalent-hydraulic model: An iron phosphate application, *J. Storage Mater.* 21 (2019) 259–271.
- [16] Q. Zhang, R.E. White, Capacity fade analysis of a lithium ion cell, *J. Power Sources* 179 (2008) 793–798.
- [17] Z.Y. Zheng, B. Chen, N. Fritz, Y. Gurumukhi, J. Cook, M.N. Ates, N. Miljkovic, P.V. Braun, P.F. Wang, Lithiation induced stress concentration for 3D metal Scaffold structured silicon anodes, *J. Electrochim. Soc.* 166 (2019) A2083–A2090.
- [18] Zheng, Z., Y. Xu, B. Chen, P. Wang, 2019, Gaussian Process Based Crack Initiation Modeling for Design of Battery Anode Materials. International Design Engineering Technical Conferences and Computers and Information in Engineering Conference. American Society of Mechanical Engineers.
- [19] Z. Zheng, Y. Xu, P. Wang, Uncertainty quantification analysis on mechanical properties of the structured silicon anode via surrogate models, *J. Electrochim. Soc.* 168 (2021), 040508.
- [20] S.S.Y. Ng, Y. Xing, K.L. Tsui, A naive Bayes model for robust remaining useful life prediction of lithium-ion battery, *Appl. Energy* 118 (2014) 114–123.
- [21] S. Cheng, M.H. Azarian, M.G. Pecht, Sensor systems for prognostics and health management, *Sensors* 10 (2010) 5774–5797.
- [22] L. Wu, X. Fu, Y. Guan, Review of the remaining useful life prognostics of vehicle lithium-ion batteries using data-driven methodologies, *Appl. Sci.* 6 (2016) 166.
- [23] W. Cao, S.L. Wang, C. Fernandez, C.Y. Zou, C.M. Yu, X.X. Li, A novel adaptive state of charge estimation method of full life cycling lithium-ion batteries based on the multiple parameters optimization, *Energy Sci. Eng.* 7 (2019) 1544–1556.
- [24] S.L. Wang, C. Fernandez, L. Shang, Z. Li, H. Yuan, An integrated online adaptive state of charge estimation approach of high-power lithium-ion battery packs, *Trans. Instit. Measure. Control* 40 (2017) 1892–1910.
- [25] J. Kim, H. Chun, M. Kim, J. Yu, K. Kim, T. Kim, S. Han, Data-driven state of health estimation of Li-ion batteries with RPT-reduced experimental data, *IEEE Access* 7 (2019) 106987–106997.
- [26] M. Kim, S. Han, Novel data-efficient mechanism-agnostic capacity fade model for Li-ion batteries, *IEEE Trans. Ind. Electron.* 68 (2021) 6267–6275.
- [27] C. Jiang, S. Wang, B. Wu, C. Fernandez, X. Xiong, J. Coffie-Ken, A state of charge estimation method of the power lithium-ion battery in complex conditions based on adaptive square root extended Kalman Filter, *Energy* 219 (2021).
- [28] S.L. Wang, C.M. Yu, C. Fernandez, M.J. Chen, G.L. Li, X.H. Liu, Adaptive state of charge estimation method for an aeronautical lithium-ion battery pack based on a reduced particle-unscented kalman filter, *J. Power Electron.* 18 (2018) 1127–1139.
- [29] G.X. Bai, P.F. Wang, C. Hu, A self-cognizant dynamic system approach for prognostics and health management, *J. Power Sources* 278 (2015) 163–174.
- [30] G.X. Bai, P.F. Wang, C. Hu, M. Pecht, A generic model-free approach for lithium-ion battery health management, *Appl. Energy* 135 (2014) 247–260.
- [31] X. Li, J. Miao, J. Ye, Lithium-ion battery remaining useful life prediction based on grey support vector machines, *Adv. Mech. Eng.* 7 (2015), 1687814015622327.
- [32] J. Qu, F. Liu, Y. Ma, J. Fan, A neural-network-based method for RUL prediction and SOH monitoring of lithium-ion battery, *IEEE Access* 7 (2019) 87178–87191.
- [33] P. Khumprom, N. Yodo, A data-driven predictive prognostic model for lithium-ion batteries based on a deep learning algorithm, *Energies* 12 (2019) 660.
- [34] Y. Duan, J. Tian, J. Lu, C. Wang, W. Shen, R. Xiong, Deep neural network battery impedance spectra prediction by only using constant-current curve, *Energy Storage Mater.* (2021) pp.
- [35] J. Yu, State of health prediction of lithium-ion batteries: multiscale logic regression and Gaussian process regression ensemble, *Reliab. Eng. Syst. Saf.* 174 (2018) 82–95.
- [36] G.E. Karniadakis, I.G. Kevrekidis, L. Lu, P. Perdikaris, S. Wang, L. Yang, Physics-informed machine learning, *Nat. Rev. Phys.* (2021) 1–19.
- [37] R.G. Nascimento, F.A. Viana, Cumulative damage modeling with recurrent neural networks, *AIAA J.* 58 (2020) 5459–5471.
- [38] M. Raissi, A. Yazdani, G.E. Karniadakis, Hidden fluid mechanics: learning velocity and pressure fields from flow visualizations, *Science* 367 (2020) 1026–1030.
- [39] L. Yang, X. Meng, G.E. Karniadakis, B-PINNs: Bayesian physics-informed neural networks for forward and inverse PDE problems with noisy data, *J. Comput. Phys.* 425 (2021), 109913.
- [40] S. Spigler, M. Geiger, S. d'Ascoli, L. Sagun, G. Birol, M. Wyart, A jamming transition from under-to over-parametrization affects generalization in deep learning, *J. Phys. A: Math. Theor.* 52 (2019), 474001.
- [41] Tu, H., S. Moura, H. Fang, Integrating Electrochemical Modeling with Machine Learning for Lithium-Ion Batteries, arXiv preprint arXiv:2103.11580, Vol. 2021, pp.

- [42] M. Aykol, C.B. Gopal, A. Anapolsky, P.K. Herring, B. van Vlijmen, M.D. Berliner, M.Z. Bazant, R.D. Braatz, W.C. Chueh, B.D. Storey, Perspective—combining physics and machine learning to predict battery lifetime, *J. Electrochem. Soc.* 168 (2021), 030525.
- [43] R.D. Deshpande, D.M. Bernardi, Modeling Solid-Electrolyte Interphase (SEI) fracture: coupled mechanical/chemical degradation of the lithium ion battery, *J. Electrochem. Soc.* 164 (2017) A461–A474.
- [44] A. Wang, S. Kadam, H. Li, S. Shi, Y. Qi, Review on modeling of the anode solid electrolyte interphase (SEI) for lithium-ion batteries, *npj Comput. Mater.* 4 (2018) 1–26.
- [45] H. Ekström, G. Lindbergh, A model for predicting capacity fade due to SEI formation in a commercial graphite/LiFePO₄ cell, *J. Electrochem. Soc.* 162 (2015) A1003.
- [46] J. Tian, R. Xiong, W. Shen, J. Lu, X.G. Yang, Deep neural network battery charging curve prediction using 30 points collected in 10 minutes, *Joule* 5 (2021) 1521–1534.
- [47] MdS. Hosen, R. Youssef, T. Kalogiannis, J. Van Mierlo, M. Berecibar, Battery cycle life study through relaxation and forecasting the lifetime via machine learning, *J. Energy Storage* 40 (2021).